JPE 3-2-6

Advanced Simulation Model for Brushless DC Motor Drives

[1]Byoung-Kuk. Lee[*] and [2]Mehrdad Ehsani

[1]Korea Electrotechnology Research Institute (KERI), Korea
[2]Dept. of Electrical Eng., Texas A&M University, College Station, USA

ABSTRACT

An advanced simulation model for brushless dc (BLDC) motor drives using Matlab is presented. In the developed model, the dynamic characteristics of speed and torque as well as voltages and currents of pwm inverter components can be effectively monitored and analyzed. Therefore, it can be expected that the developed simulation model can be an easy-to-design tool for the development of BLDC motor drives including control algorithms and topological variations with reduced computation time and memory size.

Keywords: Brushless DC Motor, Simulation, Switching Function

1. Introduction

Brushless dc (BLDC) motor drives are becoming widely used in various consumer and industrial systems, such as servo motor drives, home appliances, computer peripherals, and automotive applications[1]-[5]. Conseque ntly, many machine design and control schemes have been developed to enhance the performance of BLDC motor drives[6]-[8]. In general, the overall system consists of three parts: 1) power conversion pwm inverters, 2) BLDC motor and load, and 3) speed, torque, and current controllers. Therefore, exact understanding of each part is a prerequisite for analysis and prediction of the overall system operation.

Until now, several simulation models have been proposed for the analysis of BLDC motor drives.

These models are based on state-space equations, Fourier-series, and d-q axis model[9]-[12]. Even though the previous works made a great contribution to analysis of BLDC motor drives, to the best our knowledge, no unified approach for modeling and analysis of three parts of the drive has been proposed. In [11], the authors proposed a model by means of state array matrices to simulate the drive system along with pwm inverter. However, in addition to its inherent complexity, detailed investigation of the inverter is not concluded in this work.

In this paper, we propose a simulation model for an entire BLDC motor drive and its actual implementation. In this model, the trapezoidal back EMF waveforms are modeled as a function of rotor position, so that it can be actively calculated according to the operating speeds. Moreover, switching function concept is adopted to model the pwm inverter. This in turns results in obtaining the detailed voltage and current waveforms of the inverter and calculating the design parameters, such as average/rms ratings of components[13]-[17]. The developed model can produce precise prediction of drive performance during

transient as well as steady state operation. Therefore, the mechanism of phase commutation and generation of torque ripple can be observed and analyzed in this model. Especially, the proposed model is made into several functional modular blocks, so that it can be easily extended to other ac motor applications with a little modification, such as the induction motor, the permanent magnet ac motor, and the synchronous reluctance motor.

Therefore, it can be expected that the developed simulation model can be an easy-to-design tool for the development of BLDC motor drives including control algorithms and topological variations with reduced computation time and memory size.

2. Analysis of BLDC Motor Drive System

Fig. 1 shows the overall system configuration of the three-phase BLDC motor drive. The pwm inverter topology is six-switch voltage-source configuration with constant dc-link voltage (V_d), which is identical with the induction motor drives and the permanent magnet ac motor drives. The analysis is based on the following assumption for simplification[12]:

The motor is not saturated.

Stator resistances of all the windings are equal and self and mutual inductances are constant.

Power semiconductor devices in the inverter are ideal.

Iron losses are negligible.

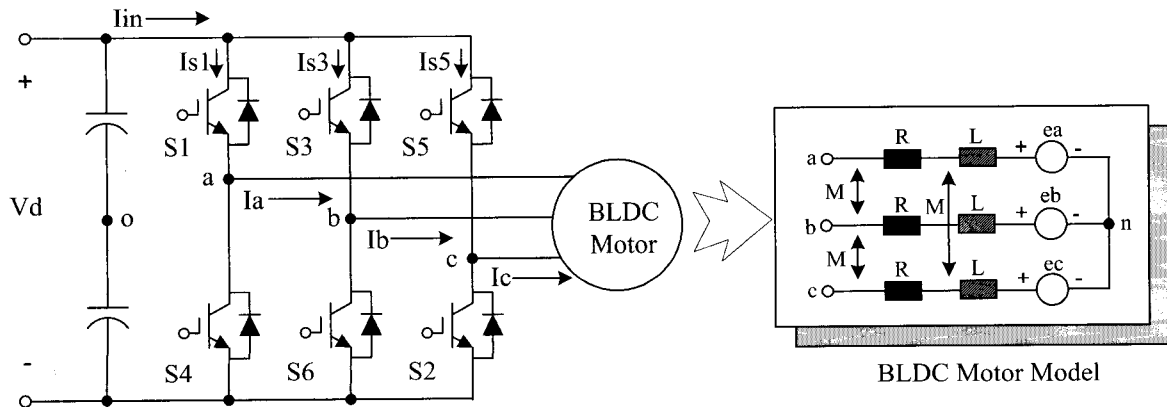Under the above assumptions, a BLDC motor can be represented as

$$\begin{bmatrix} v_a \\ v_b \\ v_c \end{bmatrix} = \begin{bmatrix} R & 0 & 0 \\ 0 & R & 0 \\ 0 & 0 & R \end{bmatrix} \begin{bmatrix} i_a \\ i_b \\ i_c \end{bmatrix} + \begin{bmatrix} L-M & 0 & 0 \\ 0 & L-M & 0 \\ 0 & 0 & L-M \end{bmatrix} \frac{d}{dt} \begin{bmatrix} i_a \\ i_b \\ i_c \end{bmatrix} + \begin{bmatrix} e_a \\ e_b \\ e_c \end{bmatrix} \quad (1)$$

where e_a, e_b and e_c are trapezoidal back EMFs.

The electromagnetic torque is expressed as

$$T_e = \frac{1}{\omega_r}(e_a i_a + e_b i_b + e_c i_c) \quad (2)$$

And, the interaction of T_e with the load torque determines how the motor speed builds up:

$$T_e = T_L + J\frac{d\omega_r}{dt} + B\omega_r \quad (3)$$

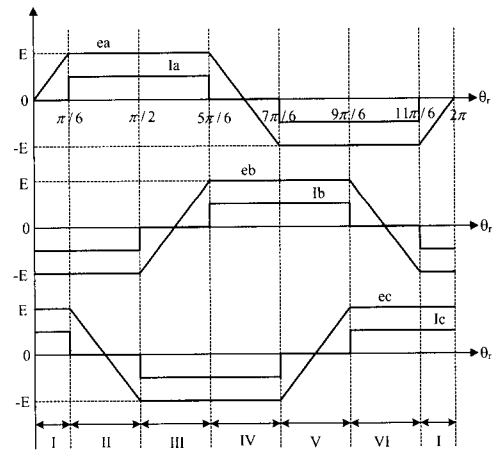where T_L is load torque, J is inertia, and B is damping.

Fig. 2. Back EMF and phase current waveforms of BLDC motor drive.

Fig. 1. Configuration of BLDC motor drive system.

(a) Mode I (I_a=0, I_b<0, I_c>0)   (b) Mode II (I_a>0, I_b<0, I_c=0)   (c) Mode III (I_a>0, I_b=0, I_c<0)

(d) Mode IV (I_a=0, I_b>0, I_c<0)   (e) Mode V (I_a<0, I_b>0, I_c=0)   (f) Mode VI (I_a<0, I_b=0, I_c>0)
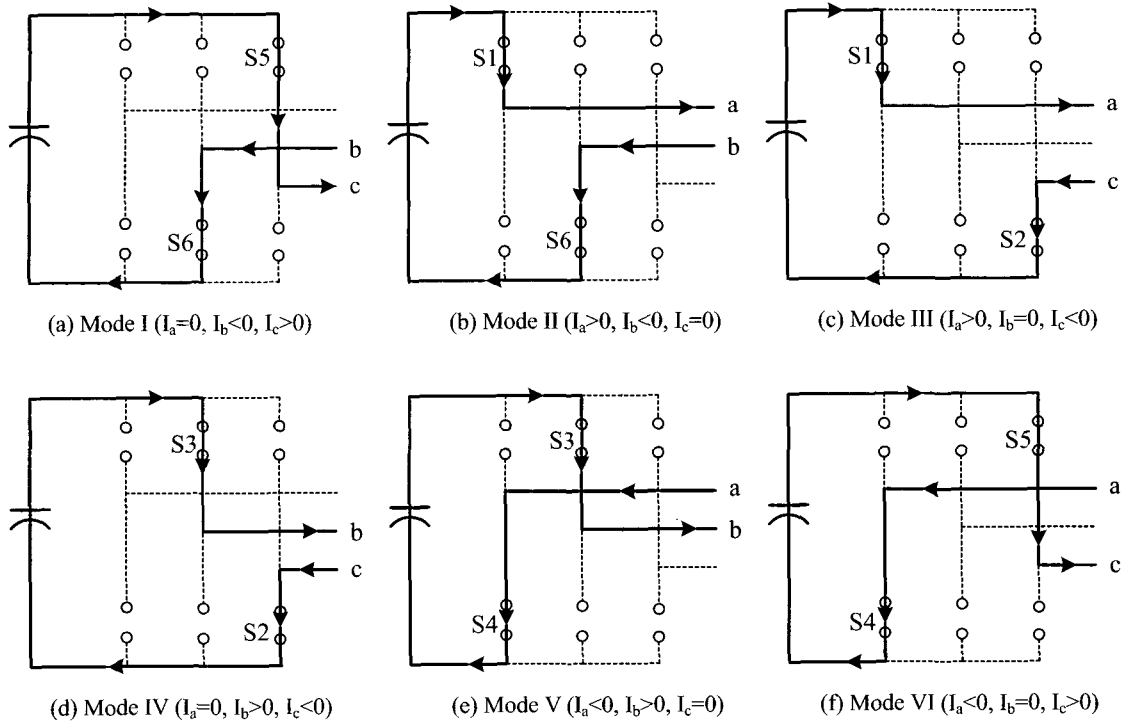
Fig. 3. Switching states and conduction sequence according to the operating modes.

The pwm three-phase inverter operation can be divided into six modes according to the current conduction states as shown in Fig. 2. The detailed switching states and conduction sequence are described in Fig. 3.

The three phase currents are controlled to take a form of quasisquare waveform in order to synchronize with the trapezoidal back EMF to produce the constant torque. This task is performed by the speed/torque control loop in cooperation with rotor position sensor and hysteresis current controller as shown in Fig. 4.
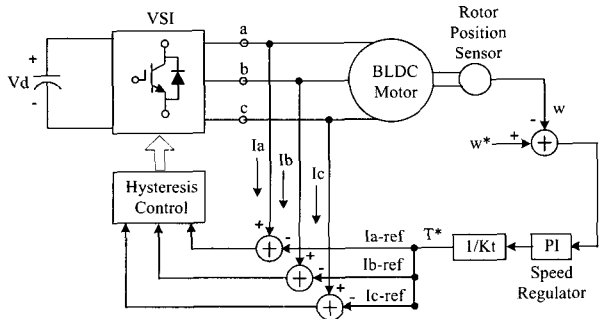

Fig. 4. Block diagram of control scheme of BLDC motor drive.

3. Modeling and Implementation

In this section, the modeling process is explained and the actual implementation using Matlab Simulink is described. Fig. 5 shows the overall block diagram of the developed model for BLDC motor drives. As shown in Fig. 5, the proposed model consists of seven functional blocks: back EMF block, load current block, hysteresis current control block, pwm inverter block, diode rectifier block, pure switch and diode currents generating block, and speed/torque controller block.

3.1 Back EMF Block

As shown in Fig. 2, the back EMF is a function of rotor position (θ_r) and has the amplitude of $E = K_e \cdot \omega_r$ (K_e is back EMF constant). In this paper, the modeling of the back EMF is performed under the assumption, such that all three phases have identical back EMF waveforms. Based on the rotor position, the numerical expression of back EMF can be obtained as eqs. (4), (5), and (6) and it is implemented as shown in Fig. 6. Therefore, with the speed
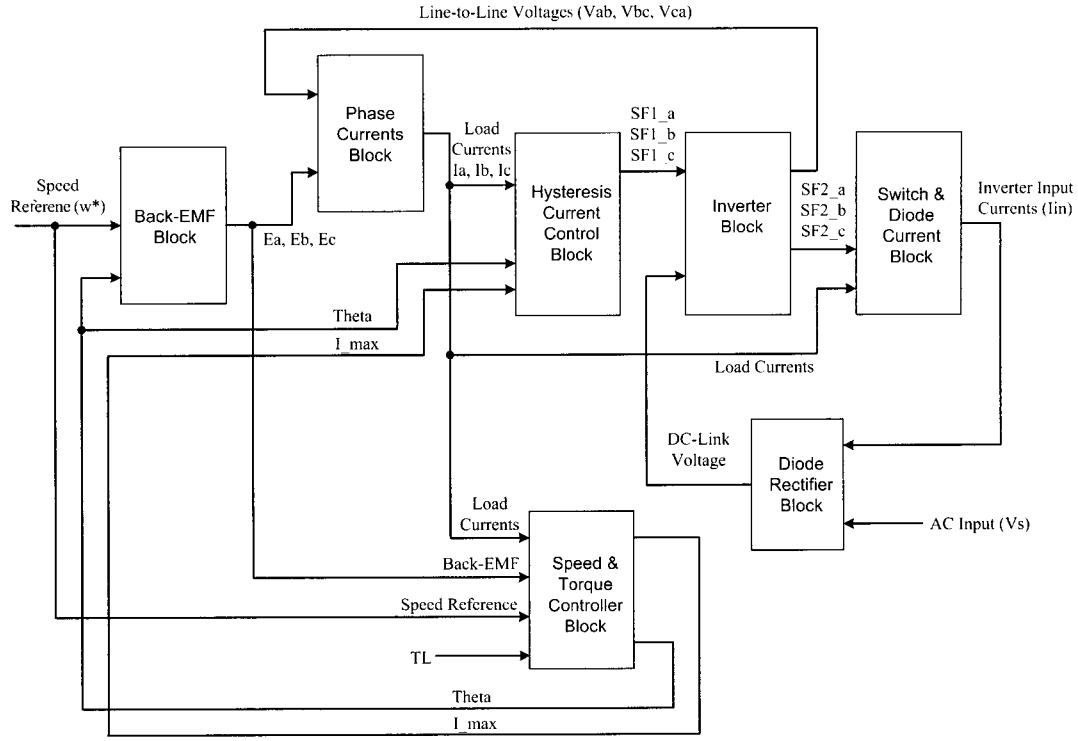
Fig. 5.   Overall block diagram of the developed model for BLDC motor drive systems.

command and rotor position, the symmetric three phases back EMF waveforms can be generated at every operating speed.

$$
e_a = \begin{bmatrix} (6E/\pi)\theta_r & (0 < \theta_r < \pi/6) \\ E & (\pi/6 < \theta_r < 5\pi/6) \\ -(6E/\pi)\theta_r + 6E & (5\pi/6 < \theta_r < 7\pi/6) \\ -E & (7\pi/6 < \theta_r < 11\pi/6) \\ (6E/\pi)\theta_r - 12E & (11\pi/6 < \theta_r < 2\pi) \end{bmatrix} \quad (4)
$$

$$
e_b = \begin{bmatrix} -E & (0 < \theta_r < \pi/2) \\ (6E/\pi)\theta_r - 4E & (\pi/2 < \theta_r < 5\pi/6) \\ E & (5\pi/6 < \theta_r < 9\pi/6) \\ -(6E/\pi)\theta_r + 10E & (9\pi/6 < \theta_r < 11\pi/6) \\ E & (11\pi/6 < \theta_r < 2\pi) \end{bmatrix} \quad (5)
$$

$$
e_c = \begin{bmatrix} E & (0 < \theta_r < \pi/6) \\ -(6E/\pi)\theta_r + 2E & (\pi/6 < \theta_r < \pi/2) \\ -E & (\pi/2 < \theta_r < 7\pi/6) \\ (6E/\pi)\theta_r - 8E & (7\pi/6 < \theta_r < 9\pi/6) \\ E & (9\pi/6 < \theta_r < 2\pi) \end{bmatrix} \quad (6)
$$

In practical situation, due to manufacturing imperfection, deterioration of permanent magnets, or unbalanced stator windings, the back EMF waveforms become unbalanced. In this case, the real back EMF could be modeled using finite element analysis (FEA).

Consequently, back EMF block can be modified by FEA program. In the next step, this data will be fed into "S-Function Block" in Matlab Simulink, which passes the program written in M, C, or Fortran to Matlab Workspace. Therefore, it is noted that the proposed model can be applied not only to the ideal back EMF case, but also to the practical case.
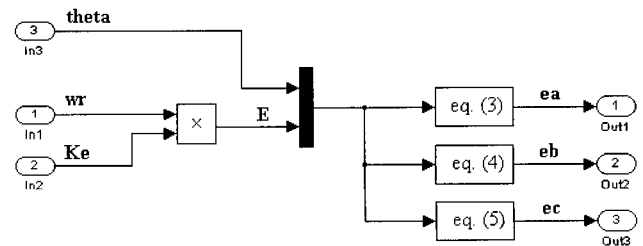

Fig. 6.   Back EMF generating block from rotor positions.

3.2 Speed and Torque Control Block

Speed and torque characteristics of the BLDC motor can be explained from eq. (3), neglecting the damping factor as

$$\omega_r = \frac{1}{J}\int (T_e - T_L)dt = \frac{1}{J}\int [(T_a + T_b + T_c) - T_L]dt \qquad (7)$$

And, the relation between electrical power (P_e) and mechanical power (P_m) is

$$P_e = EI_{max} = P_m = T_e\omega_r \qquad (8)$$

Also, torque can be controlled very directly by varying the current amplitude as

$$T_e = \frac{E}{\omega_r}I_{max} = K_t I_{max}, \quad (K_t = \frac{E}{\omega_r} = \frac{K_e\omega_r}{\omega_r} \approx K_e) \qquad (9)$$

where K_t is torque constant.

Therefore, using eqs. (7), (8) and (9), the speed and torque control circuit can be implemented as shown in Fig. 7. In this model, from the rotor speed (ω_r), the rotor position (θ_r) is converted to vary from 0 to 2π per electrical cycle. And, it is fed to back EMF block and used as data to calculate the proper back EMF waveforms. The converted rotor position can be obtained using a Matlab function, "Floor", which is rounds the element to the nearest integers as

$$f(u) = u[1] - [floor(u[1]/2\pi) \cdot 2\pi] \qquad (10)$$
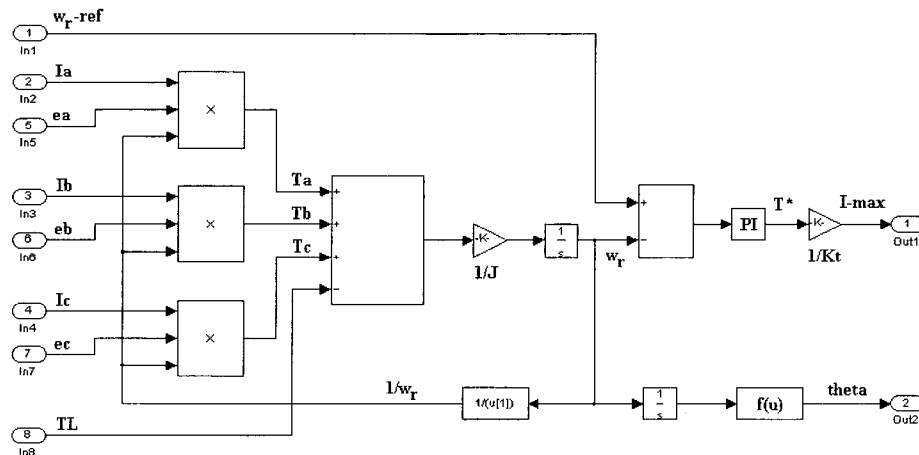
where $u[1]$ is rotor position.

3.3 Hysteresis Current Control Block

In BLDC motor drive, duty-cycle controlled voltage pwm technique and hysteresis current control technique can be regarded as the main current control strategies. In this paper, bipolar hysteresis current control is used for obtaining the fast dynamic responses during transient states. This current control method is explained based on the case of phase A. As shown in Fig. 8(a), current control for phase A can be divided into each four-period as following the polarity of the current:

(1) Case I: $I_a > 0$

Period 1: $I_a < Lower\ Limit(LL) \rightarrow$ Switch S_1 is turned on.

Period 2: $I_a < Upper\ Limit(UL) \rightarrow$ Switch S_1 is turned off and D_4 is conducted.

Period 3: $LL < Ia < UL\ and\ dI_a/dt > 0 \rightarrow S_1$ is turned on.

Period 4: $LL < Ia < UL\ and\ dI_a/dt < 0 \rightarrow$ Switch S_1 is turned off and D_4 is conducted.
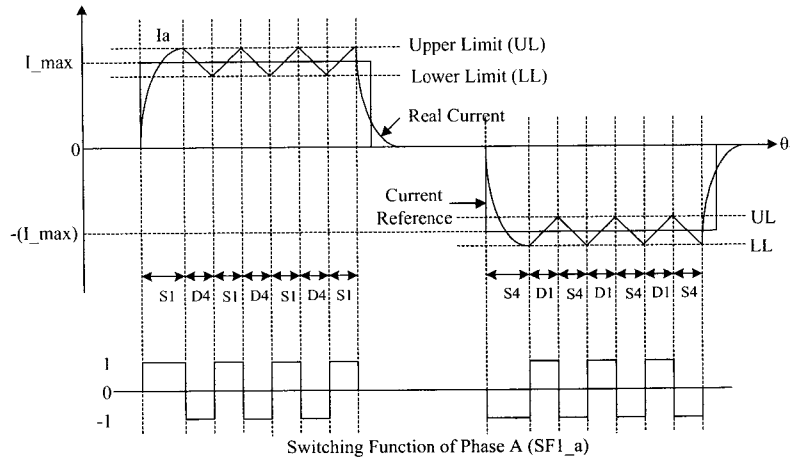
(2) Case II: $I_a < 0$

Period 1: $I_a > UL \rightarrow$ Switch S_4 is turned on.

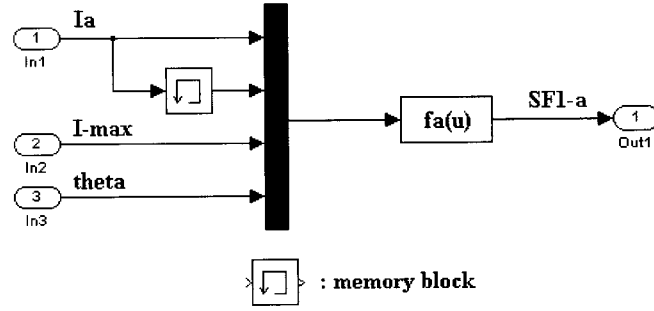Period 2: $I_a < LL \rightarrow$ Switch S_4 is turned off and D_1 is conducted.

Period 3: $LL < Ia < UL\ and\ dI_a/dt < 0 \rightarrow S_4$ is turned on.

Period 4: $LL < Ia < UL\ and\ dI_a/dt > 0 \rightarrow$ Switch S_4 is turned off and D_1 is conducted.

Fig. 7.   Speed and torque control block.

(a)

(b)

Fig. 8.   (a) Detailed investigation of hysteresis current control for phase A, and (b) its implementation.

$$
f_a(u) = (u[4] > \pi/6) \cdot (u[4] < 5\pi/6) \cdot \begin{bmatrix} (u[1] < u[3]*0.9) - (u[1] > u[3]*1.1) + \\ (u[1] > u[3]*0.9)*(u[1] < u[3]*1.1)*(u[1] > u[2]) - \\ (u[1] > u[3]*0.9)*(u[1] < u[3]*1.1)*(u[1] < u[2]) \end{bmatrix} +
$$

$$
(u[4] > 7\pi/6) \cdot (u[4] < 11\pi/6) \cdot \begin{bmatrix} -(u[1] > -u[3]*0.9) + (u[1] < -u[3]*1.1) - \\ (u[1] < -u[3]*0.9)*(u[1] > -u[3]*1.1)*(u[1] < u[2]) + \\ (u[1] < -u[3]*0.9)*(u[1] > -u[3]*1.1)*(u[1] > u[2]) \end{bmatrix}
$$

(11)

This hysteresis current control logic is realized in a function block $f_a(u)$ in cooperation with the measured phase A current I_a, current reference I_{max}, and rotor position θ_r as shown in Fig. 8(b), such as form (11), where,

u[1] is the measured I_a,

u[2] is the previous value of I_a,

u[3] is the maximum value of current reference (I_max),

u[4] is the rotor position (θ_r),

u[3]*0.9 is the lower limit,

u[3]*1.1 is the upper limit.

From the hysteresis block, the switching function SF_{1_a}, SF_{1_b}, and SF_{1_c} are determined to model the operation of pwm inverter. The switching function concept is a powerful tool in understanding and optimizing the performance of the static power converters/inverters[13]-[17]. Using the switching function concept, the power conversion circuits can be modeled according to their functions, rather than circuit topologies. Therefore, it can achieve simplification of the overall power conversion functions, so that the convergence and long-run time problems, which are common in PSPICE and SABER, can be solved[17].

In this model, the switching function SF_1 is used to generate the inverter line-to-line voltages. Also, it is modified to SF_2 for obtaining the pure switch and diode currents according to the switching states. Consequently, using switching functions (SF_1 and SF_2), the detailed inverter operation under hysteresis current control can be effectively expressed.

3.4 PWM Inverter, Load Current and Pure Switch/Diode Current Blocks

As shown in Fig. 3, the only two phases are excited through the conduction operating modes. Therefore, the three phases currents are considered in terms of the line-to-line voltages. From Fig. 9, the following voltage and current equations can be obtained as

$$
\begin{cases}
v_{ab} = R_{LL}i_1 + (L-M)_{LL}\dfrac{di_1}{dt} + e_{ab} \\[2mm]
v_{bc} = R_{LL}i_2 + (L-M)_{LL}\dfrac{di_2}{dt} + e_{bc} \\[2mm]
v_{ca} = R_{LL}i_3 + (L-M)_{LL}\dfrac{di_3}{dt} + e_{ca}
\end{cases}
\tag{12}
$$

where, R_{LL} is the line-to-line resistance and equals to $2R$,

(L - M)$_{LL}$ is the line-to-line inductance and equals to $2(L-M)$,

e_{ab}, e_{bc} and e_{ca} are the line-to-line back EMFs and $e_{ab} = e_a - e_b$, $e_{bc} = e_b - e_c$ and $e_{ca} = e_c - e_a$.

And,

$$
\begin{cases}
i_a = i_1 - i_3 \\
i_b = i_2 - i_1 \\
i_c = i_3 - i_2
\end{cases}
\tag{13}
$$

Using switching function $SF_{1\_a,b,c}$, which is obtained from hysteresis block, the V_{ao}, V_{bo}, and V_{co} can be calculated as

$$
\begin{cases}
v_{ao} = \dfrac{V_d}{2}SF_{1\_a} = \dfrac{V_d}{2}\sum_0^\infty A_n \sin(n\omega t) \\[2mm]
v_{bo} = \dfrac{V_d}{2}SF_{1\_b} = \dfrac{V_d}{2}\sum_0^\infty A_n \sin n(\omega t - 120^\circ) \\[2mm]
v_{co} = \dfrac{V_d}{2}SF_{1\_c} = \dfrac{V_d}{2}\sum_0^\infty A_n \sin n(\omega t - 240^\circ)
\end{cases}
\tag{14}
$$

Then, the inverter line-to-line voltages can be derived as

$$
\begin{cases}
v_{ab} = v_{ao} - v_{bo} = \dfrac{V_d}{2}(SF_{1\_a} - SF_{1\_b}) \\[2mm]
v_{bc} = v_{bo} - v_{co} = \dfrac{V_d}{2}(SF_{1\_b} - SF_{1\_c}) \\[2mm]
v_{ca} = v_{co} - v_{ao} = \dfrac{V_d}{2}(SF_{1\_c} - SF_{1\_a})
\end{cases}
\tag{15}
$$

Next, the three phases currents are obtained solving the eqs. (12) and (13). From the calculated phase currents, the detailed pure switch and diode currents are derived using switching function SF_2. Each phase has two switching functions of SF_2, such as SF_{2_S1} and SF_{2_S4} for switches S_1 and S_4, respectively with the following definition as

$$
\begin{cases}
SF_{2\_S1} = SF_{1\_a} > 0 \\
SF_{2\_S4} = SF_{1\_a} < 0
\end{cases}
\tag{16}
$$

Based on the eq. (16) and Fig. 8(a), the switch and diode currents for phase A are calculated as

$$
\begin{cases}
I_{S1\_S} = (I_a > 0)\cdot SF_{2\_S1} \\
I_{S1\_D} = (I_a < 0)\cdot SF_{2\_S1} \\
I_{S4\_S} = (I_a < 0)\cdot SF_{2\_S4} \\
I_{S1\_D} = (I_a > 0)\cdot SF_{2\_S4}
\end{cases}
\tag{17}
$$

where, I_{S1_S} and I_{S1_D} are pure switch and diode currents of switch S_1 as $I_{S1} = I_{S1\_S} - I_{S1\_D}$, I_{S4_S} and I_{S4_D} are pure switch and diode currents of switch S_4 as $I_{S4} = I_{S4\_S} - I_{S4\_D}$.
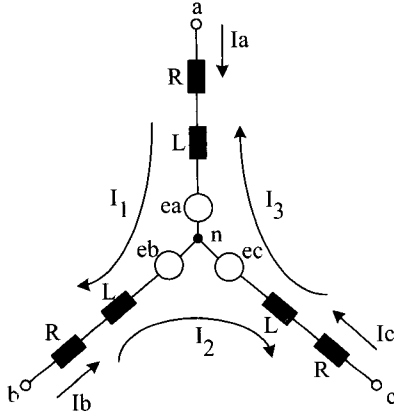
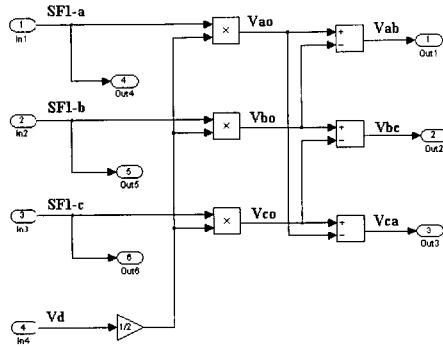Fig. 9. Voltage and current parameters in three-phase BLDC motor.

Fig. 10. Inverter line-to-line voltage generating block using switching functions.

Also, the inverter input current (I_{in}) can be obtained by

$$I_{in} = I_{S1} + I_{S3} + I_{S5} \qquad (18)$$

Finally, the average and rms values of current parameters can be expressed by the vector forms such as eqs. (19) and (20) and it can be calculated in Matlab workspace by getting the data from Fig. 5.

$$I_{S1\_S,avg} = \frac{1}{T}\int_0^T I_{S1\_S}(t)dt = \frac{1}{2n}\sum_{k=1}^{n}\left[I_{S1\_S}(k) + I_{S1\_S}(k-1)\right] \qquad (19)$$

$$I_{S1\_S,rms} = \sqrt{\frac{1}{T}\int_0^T I_{S1\_S}{}^2(t)dt} = \sqrt{\frac{1}{2n}\sum_{k=1}^{n}\left[I_{S1\_S}{}^2(k) + I_{S1\_S}{}^2(k-1)\right]} \qquad (20)$$

The implementations of the above-explained numerical pwm inverter voltage and current equations are shown in Fig. 10, Fig. 11, and Fig. 12. Consequently, from the

inverter, load current, and switch/diode blocks, all voltage and current variables of the pwm inverter can be obtained.
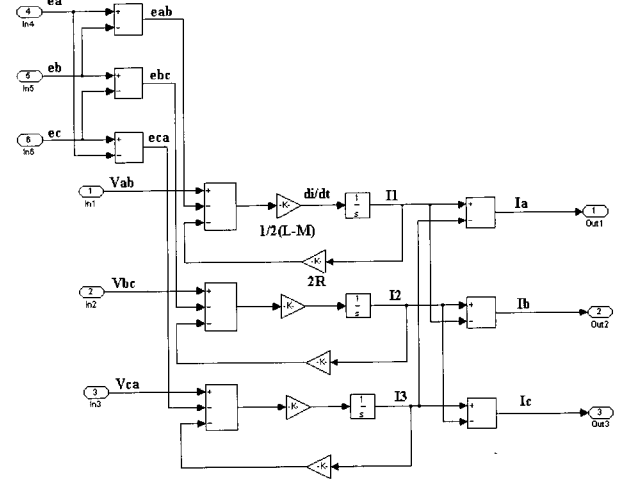

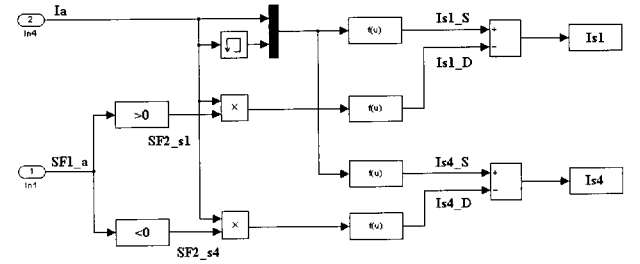Fig. 11. Implementation of three-phase currents block.

Fig. 12. Pure switch and diode currents generating block for phase A.

4. Simulation and Experimental Results

Table 1 shows the BLDC motor specification to examine the performance of the proposed model.

Table 1. Motor Specification (LL: line-to-line).

| K_t	0.21476[Nm]	R_{LL}	1.5[Ω]
K_{e_LL}	0.21486[V/(rad/sec)]	$(L-M)_{LL}$	6.1[mH]
J	8.2614e-5[kgm²]	Power	1[HP]
T_L	0.662[Nm]	Rated Speed	3500[rpm]

Fig. 13 shows the generated back EMF from the rotor position and the phase currents waveforms according to the each operating speed, such as 2500[rpm] and 3500[rpm]. As shown in Fig. 13, the three-phase symmetric back EMF waveforms are actively calculated and generated from the rotor position. At 2500[rpm], the rotor position is varied from 0 to 2π per electric cycle 0.024[s] and the back EMF has the amplitude of 28.11[V]. On the other hand, at 3500[rpm], electric cycle is 0.017[s] and amplitude is 39.36[V]. Also, the actual phase currents are successfully obtained by the hysteresis control algorithm and they are well synchronized with their counterpart back EMF waveforms as explained in Section III-C. In Fig. 14, the expanded current waveforms for phase A are depicted. In these waveforms, the current

pulsation is measured at the middle of 120° conduction periods. They result from the commutation of the other two phases (phases B and C).

The detailed analysis of the torque ripple due to the commutation is well explained in [10]. Based on the simulation conditions at 3500[rpm], DC-Link voltage (160V) is larger than the value of $4E$ (157.44V), that is $V_d > 4E$. Therefore, the phase C current reaches the I_{max} value before phase B current goes to zero [10]. As the result of that, the phase A current decreased and torque becomes to be increased during the commutation period. This phenomenon can be observed in Fig. 15. Therefore, it is noted that in the developed simulation model, the transient characteristics are well examined as well as the steady state ones.
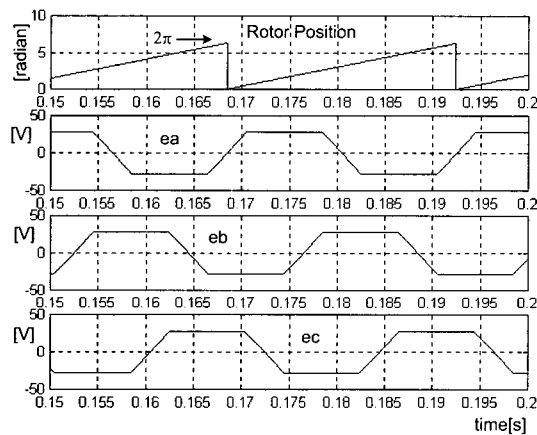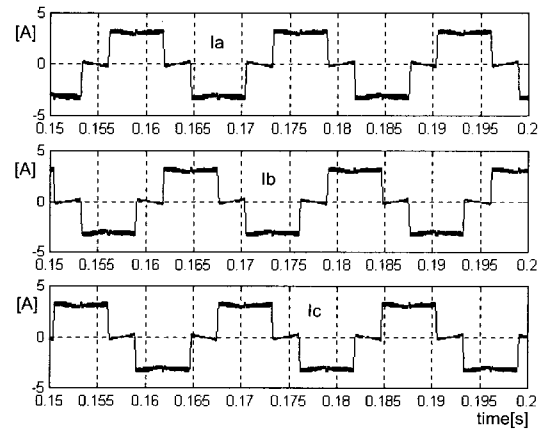

(a) At 2500[rpm]
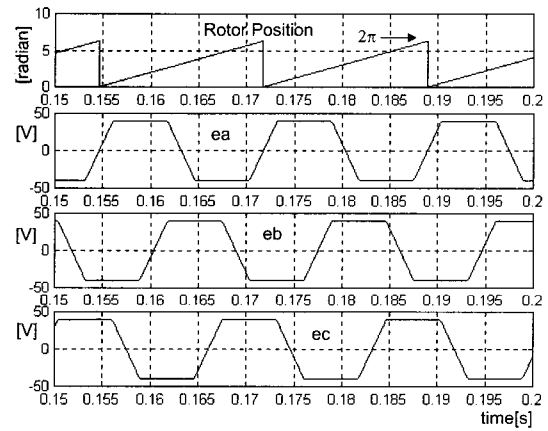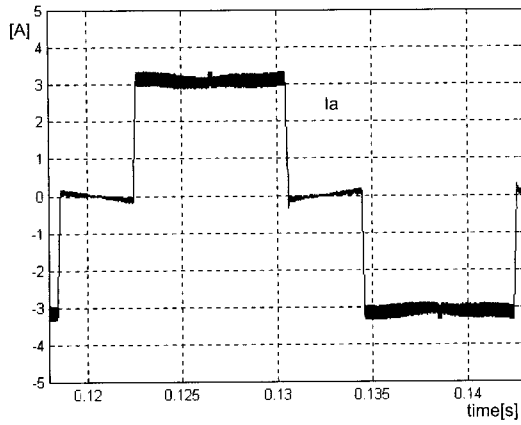

(b) At 3500[rpm]
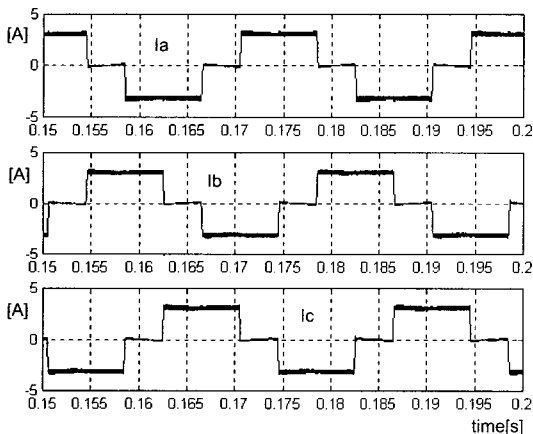
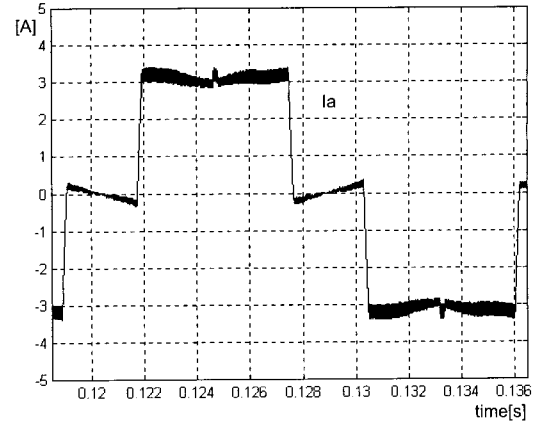(c) At 2500[rpm]

(d) At 3500[rpm]

Fig. 13.   Back EMF (upper) and phase currents (lower) waveforms based on the rotor position.
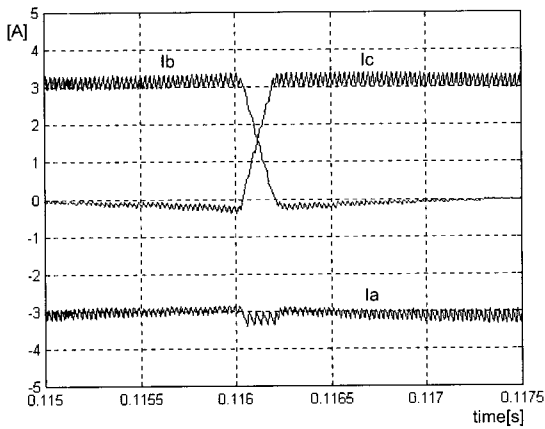
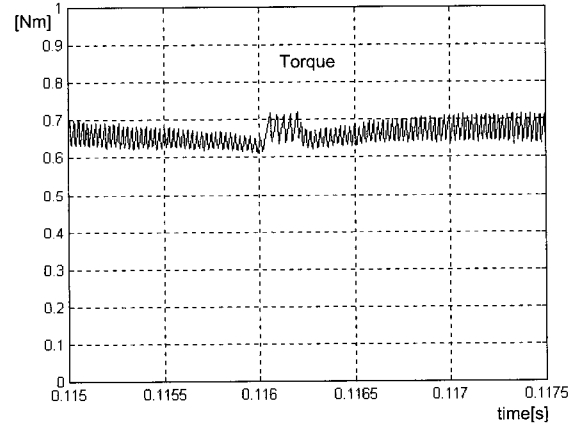(a) At 2500[rpm]   (b) At 3500[rpm]

Fig. 14.   Expanded current waveforms for phase A.
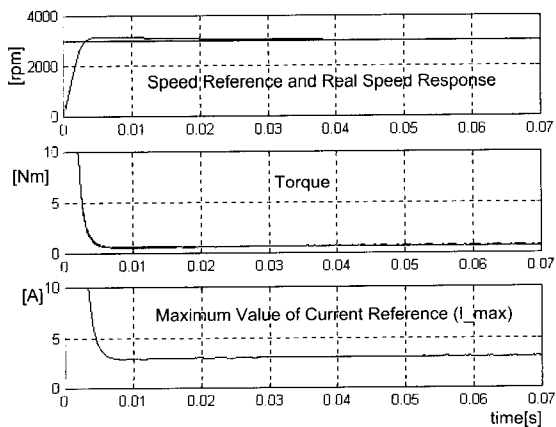

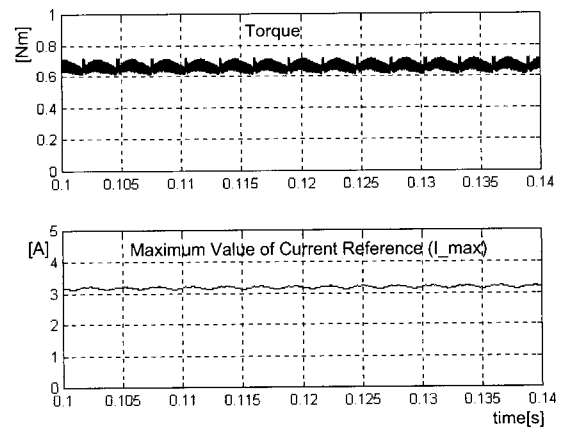(a) Phase currents   (b) Torque

Fig. 15.   Phase current and torque pulsations during the commutation period at 3500[rpm].

(a)   (b)

Fig. 16.   (a) Dynamic responses of speed and torque controller. (b) Expanded waveforms.

Fig. 16(a) shows the dynamic responses of the speed and torque controller, which is designed as shown in Fig. 7. With the help of PI controller, the real speed is reaching to the command value in 0.02[s]. Also, from the generated constant torque reference, maximum current reference value (I_{max}) is calculated, and then it is used in the hysteresis control block. From the expanded waveform in Fig. 16(b), the torque pulsation due to the commutation can be measured and using eq. (19), the average values of torque and maximum current reference value are calculated about 0.65[Nm] and 3.15[A], respectively.

From Fig. 17 to Fig. 18, the detailed operational characteristics of the pwm inverter are examined. As explained in Section III-C and D, the pwm inverter modeling is based on switching function concept.

Fig. 17(a) and Fig. 17(b) show the switching function SF_1 for the three phases (SF_{1_a}, SF_{1_b}, SF_{1_c}). From the figures, it is noted that the switching function signals are only generated during the 120° conduction periods in order to force the currents to be switched between the hysteresis upper and lower bands. The positive (negative) value 1 (-1) expresses the upper (lower) switch or diode is under the conducting state. Therefore, from the switching function SF_1, the line-to-line voltage waveforms can be obtained. Fig. 17(c) and Fig. (d) show the generated line-to-line voltage (V_{ab}) according to the conduction modes. In case of Fig. 17(c), phase A current is positive and phase B current is negative, which is mode II in Fig. 3. Therefore, during positive slope of phase A ($di_a/dt>0$) and negative slope of phase B ($di_b/dt<0$), switches S_1 and S_6

Table 2. V_{ab} and Conducting Devices according to the Current States

V_{ab} and Conducting Devises			Ia			
			>0		<0	
			$di_a/dt>0$	$di_a/dt<0$	$di_a/dt>0$	$di_a/dt<0$
Ib	>0	$di_b/dt>0$	×	×	×	$-V_d, S_3, S_4$
		$di_b/dt<0$	×	×	V_d, D_1, D_6	×
	<0	$di_b/dt>0$	×	$-V_d, D_3, D_4$	×	×
		$di_b/dt<0$	V_d, S_1, S_6	×	×	×

Table 3. V_{bc} and Conducting Devices according to the Current States

V_{bc} and Conducting Devices			I_b			
			>0		<0	
			$di_b/dt>0$	$di_b/dt<0$	$di_b/dt>0$	$di_b/dt<0$
I_c	>0	$di_c/dt>0$	×	×	×	$-V_d, S_5, S_6$
		$di_c/dt<0$	×	×	V_d, D_2, D_3	×
	<0	$di_c/dt>0$	×	$-V_d, D_5, D_6$	×	×
		$di_c/dt<0$	V_d, S_2, S_3	×	×	×

Table 4. V_{ca} and Conducting Devices according to the Current States

| V_{ca} and Conducting Devices			I_c			
			>0		<0	
			$di_c/dt>0$	$di_c/dt<0$	$di_c/dt>0$	$di_c/dt<0$
I_a	>0	$di_a/dt>0$	×	×	×	$-V_d, S_1, S_2$
		$di_a/dt<0$	×	×	V_d, D_4, D_5	×
	<0	$di_a/dt>0$	×	$-V_d, D_1, D_2$	×	×
		$di_a/dt<0$	V_d, S_4, S_5	×	×	×

are conducted, so that V_{ab} has positive value of V_d (160V). On the other hand, V_{ab} has negative V_d for the period of $d_{ia}/dt<0$ and $d_{ib}/dt>0$ (diodes D_4 and D_3 are conducted). The similar explanation can be applied to the case of $I_a<0$ and $I_b>0$ (mode V) as shown in Fig. 17(d). Consequently, the patterns of the line-to-line voltages (V_{ab}, V_{bc}, V_{ca}) and conducting devices according to the currents states are summarized in Tables II, III, and IV.

In order to obtain the optimal design parameters of the pwm inverter, the pure switch and diode current waveforms are necessary for calculating the average and rms values. They also can be obtained from the combination of the phase currents and switching function SF_2. Fig. 18 explains the detailed process of calculating the pure switch and diode currents.

In case of $I_a>0$, the current can be flowing through the switch S_1 or diode D_4. If the current is increased ($d_{ia}/dt>0$), the switch S_1 is turned on and the current flows through the switch S_1. Also, when the current is decreased ($d_{ia}/dt>0$), the switch S_1 is turned off and the current is conducted through the diode D_4. Switching function SF_2 for S_1 (SF_{2_S1}) and D_4 (SF_{2_S4}) are obtained from the switching function SF_{1_a}, which is explained in eq. (16). As the result of that, the pure switch and diode currents can be successfully obtained. As shown in Fig. 18(a) and (b), the only positive slope part of phase current I_a is selected as the pure switch current I_{s1_S} and the negative slope part is as the pure diode current I_{s4_D}. In case of $I_a<0$, the switch S_4 and the diode D_1 provide the current path and the pure switch current I_{s4_S} and the pure diode current
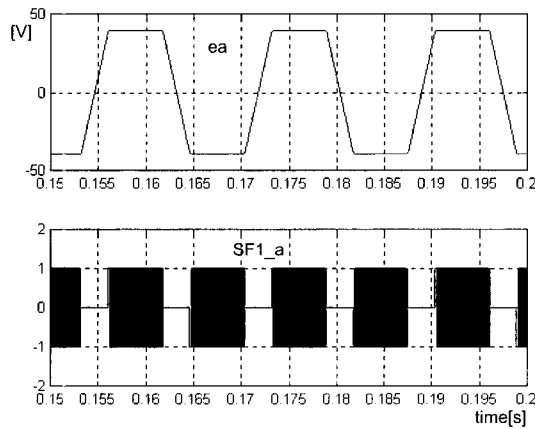
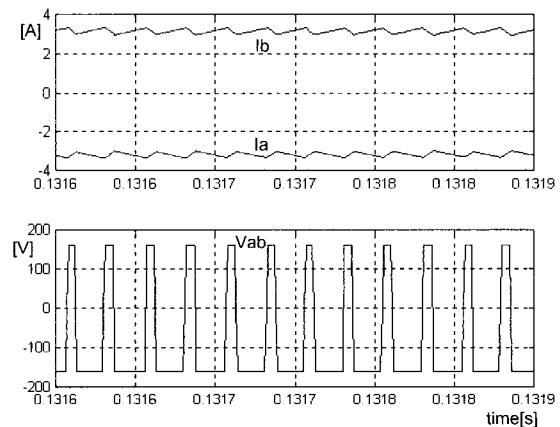(a) Back EMF and switching function for phase A
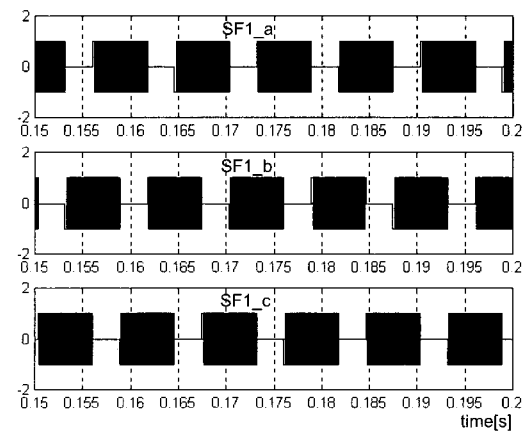
(b) Switching function SF_1
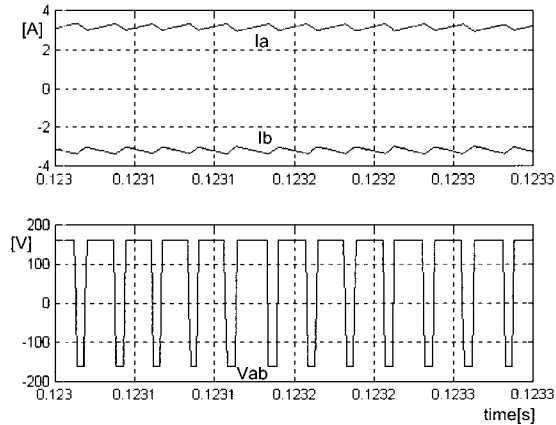
(c) Line-to-line voltage V_{ab} ($I_a>0$, $I_b<0$)

(d) Line-to-line voltage V_{ab} ($I_a<0$, $I_b>0$)

Fig. 17.   Switching function $SF_{1\_a,b,c}$ and line-to-line voltage (V_{ab}) waveforms according to the conducting modes.

I_{s1_D} can be expressed as shown in Fig. 18(d).

After obtaining the pure switch and diode current waveforms, the average and rms values can be easily calculated using eqs. (19) and (20). As an example, for S_1 and D_1, the average values are calculated as 0.657[A] and 0.240[A], respectively under the operating speed is 3500[rpm] and hysteresis window size is 10% of the maximum current reference values. Also, about rms values, one can obtain 1.415[A] and 0.871[A].

Fig. 19 shows the experimental waveforms of general three-phase BLDC motor drives. The motor specification for this test is as follows:

K_t=1.605[Nm], K_{e_LL}=1.146[V/(rad/sec)],

No. of Pole=4[Pole],

$R_{\_LL}$=7.82[Ω],

$(L-M)_{\_LL}$=77.6[mH],

Power=1[HP].

From Fig. 19(a) and Fig. 19(b), it is noted that the phase currents are synchronized with the their trapezoidal shaped back EMFs and the hysteresis current controller keeps the phase currents to follow the reference value. Switching function signals for phases A and B are displayed in Fig. 19(c). This result has a good agreement with the theoretical explanation and the simulation results as explained in the previous sections.
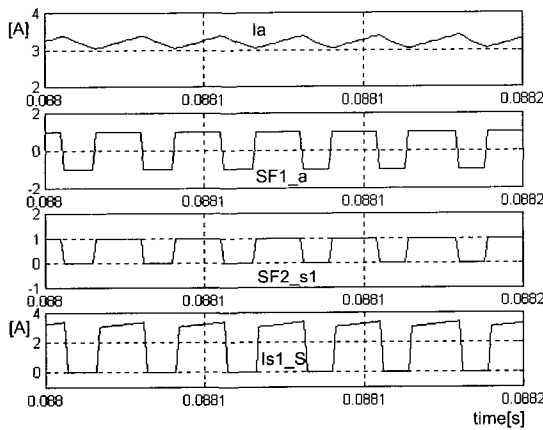
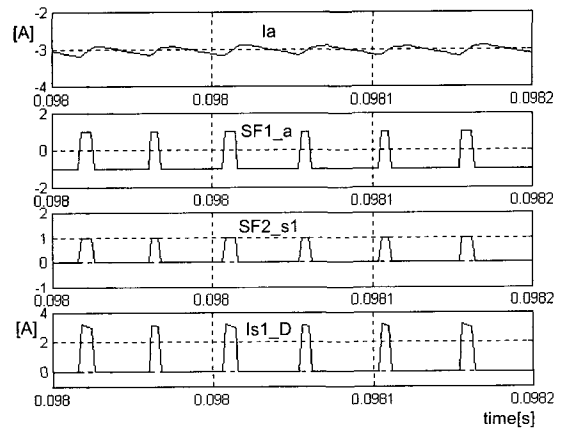(a) Pure switch current I_{s1_S} (I_a>0)
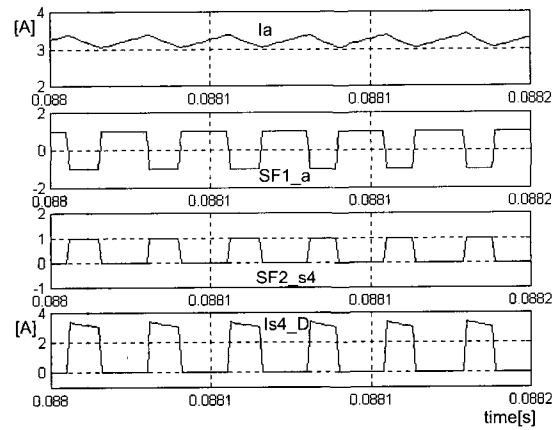
(b) Pure diode currents I_{s4_D} (I_a>0)
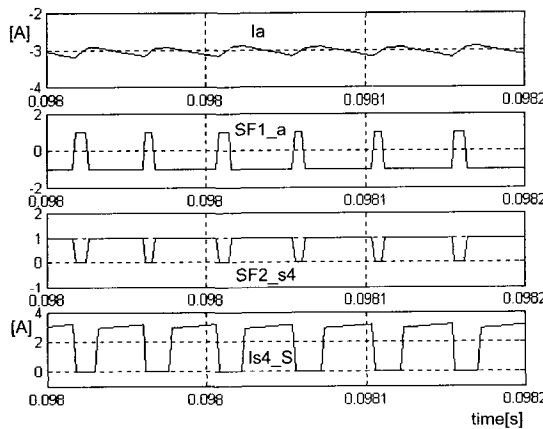
(c) Pure switch current I_{s4_S} (I_a<0)

(d) Pure diode currents I_{s1_D} (I_a<0)

Fig. 18. Pure switch and diode current waveforms of switch S_1.

(a) Back EMFs (20ms/div.; 50V/div.)

(b) Phase currents (20ms/div.; 5A/div.)

(c) Phase currents and switching signals (5ms/div.; 2A/div.; 10V/div.)

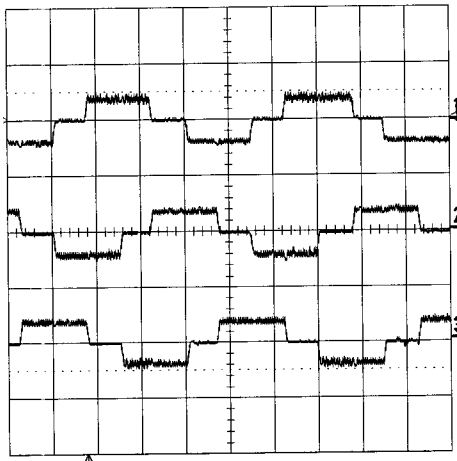Fig. 19. Experimental waveforms of BLDC motor drives .

5. Conclusions

In this paper, an advanced simulation model for BLDC motor drives are proposed and the performance and feasibilities have been examined by the informative simulation verification. From the investigation of the developed simulation model, it is expected that the dynamic characteristics as well as steady state can be effectively monitored and predicted, so that the performance of a developed system can be more precisely analyzed according to the variation of control algorithm and topology.

References

[1] A. Kusko and S. M. Peeran, "Definition of the Brushless DC Motor", in Conf. Rec. IEEE-IAS, pp. 20~22, 1988.

[2] J. R. Hendershot and T. J. E. Miller, "Design of Brushless Permanent-Magnet Motor", Oxford : Oxford Science, 1994.

[3] T. Kenjo and S. Nagamori, "Permanent Magnet and Brushless DC Motors", Tokyo : Sogo Electronics, 1984.

[4] D. C. Hanselman, "Brushless Permanent-Magnet Motor Design", New York : McGraw-Hill, 1994.

[5] T. M. Jahns, "Motion Control with Permanent-Magnet AC Machines", in IEEE Proc., Vol. 82, No. 8, pp. 1241~1252, 1994.

[6] T. A. Lipo and F. G. Turnbull, "Analysis and Comparison of Two Types of Square-Wave Inverter Drives", IEEE Trans. on Industry Applications, Vol. 11, No. 2, pp. 137~147, March/April 1975.

[7] T. M. Jahns and W. L. Soong, "Pulsating Torque Minimization Techniques for Permanent Magnet AC Motor Drives-A Review", IEEE Trans. on Industry Applications, Vol. 43, No. 2, pp. 321~330, April 1996.

[8] J. P. Johnson and M. Ehsani, "Review of Sensorless Methods for Brushless DC", in Conf. Rec. IEEE-IAS, pp. 143~150, 1999.

[9] P. Pillay and R. Krishnan, "Modeling, Simulation, and Analysis of Permanent-Magnet Motor Drives, Part II: the Brushless DC Motor Drive", IEEE Trans. on Industry Applications, Vol. 25, No. 2, pp. 274~279, March/April 1989.

[10] R. Carlson, M. Lajoie-Mazenc and C. dos S. Fagundes, "Analysis of Torque Ripple Due to Phase Commutation in Brushless DC Machines", IEEE Trans. on Industry Applications, Vol. 28, No. 3, pp. 632~638, May/June
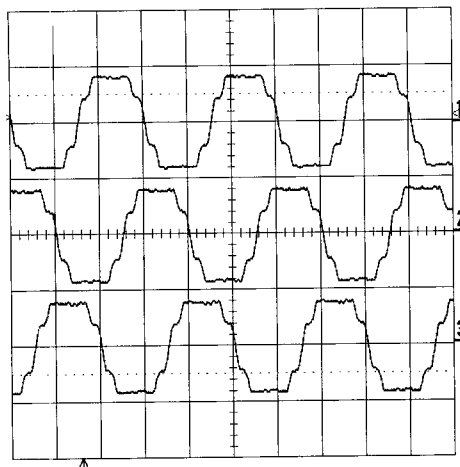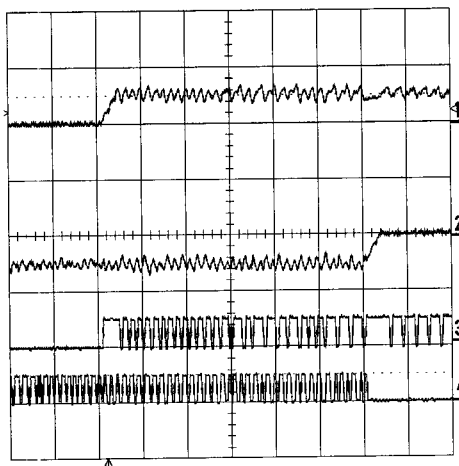
1992.

[11] P. D. Evans and D. Brown, "Simulation of Brushless DC Drives", in IEE Proc., Vol. 137, No. 5, pp. 299~308, Sep. 1990.

[12] S. K. Safi, P. P. Acarnley and A. G. Jack, "Analysis and Simulation of the High-Speed Torque Performance of Brushless DC Motor Drives", in IEE Proc., Vol. 142, No. 3, pp. 191~200, May 1995.

[13] P. Wood, "Theory of Switching Power Converter", New York : Van Nostrand-Reinhold, 1981.

[14] P. D. Ziogas, E. P. Wiechmann and V. R. Stefanovic, "A Computer-Aided Analysis and Design Approach for Static Voltage Source Inverter", IEEE Trans. on Industry Applications, Vol. IA-21, No. 5, pp. 1234~1241, Sep./Oct. 1985.

[15] E. P. Wiechmann, P. D. Ziogas and V. R. Stefanovic, "Generalized Functional Model for Three Phase PWM Inverter/Rectifier Converters", in Conf. Rec. IEEE-IAS, pp. 984~993, 1985.

[16] L. Salazar and G. Joos, "PSPICE Simulation of Three-Phase inverters by Means of Switching Functions", IEEE Trans. on Power Electronics., Vol. 9, No. 1, pp. 35~42, Jan. 1994.

[17] B. K. Lee and M. Ehsani, "A Simplified Functional Model for 3-Phase Voltage-Source Inverter Using Switching Function Concept", in Conf. Rec. IEEE-IECON, pp. 462~467, 1999.

Byoung-Kuk Lee received the B.S. and M.S. degrees from Hanyang University, Seoul, Korea in 1994 and 1996, respectively, and the Ph.D. degree from Texas A&M University, College Station, Texas in 2001, all in electrical engineering. From January 2002 to January 2003, he worked as a postdoctoral research associate at Advanced Vehicle and Motor Drives Research Center, Texas A&M University, College Station, Texas. From March 2003, he is working as a senior researcher at Korean Electrotechnology Research Institute (KERI), Changwon, Korea. His research interests include reduced parts converters and sensorless controls for brushless dc motor, induction motor, and switch reluctance motor drives, fuel cell energy conversion systems, real time simulation for power electronics and multi-converter power system, ac-dc-ac power conversion circuits, resonant power systems, and power electronics. He has served as a reviewer for the IEEE Transactions Power Electronics (PELS) and Industrial Electronics (IES) and the IEE Electronics Letters and is a member of Industrial Drive Committee (IDC) and Industrial Power Converter Committee (IPCC) of the IEEE Industry Application Society.

Mehrdad Ehsani received the Ph.D. degree from the University of Wisconsin-Madison in 1981, in electrical engineering. Since 1981 he has been at Texas A&M University, College Station, Texas where he is now a Professor of electrical engineering and Director of Advanced Vehicle Systems Research Program. He is the author of over 300 publications in pulsed-power supplies, high-voltage engineering, power electronics and motor drives, and is the recipient of the Prize Paper Award in Static Power Converters and motor drives at the IEEE-Industry Applications Society 1985, 1987, and 1992 Annual Meetings. In 1992, he was named the Halliburton Professor in the College of Engineering at A&M. In 1994, he was also named the Dresser Industries Professor in the same college. In 2001 he was named the Dow Chemical Faculty Fellow of the College of Engineering at Texas A&M University. In 2001 he also received the James R. Evans Avant Garde Award from IEEE Vehicular Technology Society. He is the recipient of IEEE Undergraduate Teaching Award for 2003. He is the co-author of two books on power electronics and motor drives and a contributor to an IEEE Guide for Self-Commutated Converters and other monographs and books. He is the author of over twenty U.S. and EC patents. His current research work is in power electronics, motor drives, hybrid electric vehicles and systems. Dr. Ehsani has been a member of IEEE Power Electronics Society AdCom, past Chairman of PELS Educational Affairs Committee, past Chairman of IEEE-IAS Industrial Power Converter Committee and past chairman of the IEEE Myron Zucker Student-Faculty Grant program. He was the General Chair of IEEE Power Electronics Specialist Conference for 1990. He is an IEEE Industrial Electronics Society and Vehicular Technology Society Distinguished Speaker and IEEE Industry Applications Society past Distinguished Lecturer. He is also the associate editor of IEEE Transactions of IES and VTS and chairman of Vehicular Technology Society Vehicle Power and Propulsion Committee. He was elected to the Board of Governors of IEEE-VTS in 2003. In 1996, he was elected Fellow of IEEE. He is also a registered professional engineer in the State of Texas.